

## ARTICLE OPEN



# Quantum emulation of the transient dynamics in the multistate Landau-Zener model

Alexander Stehli<sup>1</sup>✉, Jan David Brehm<sup>1</sup>, Tim Wolz<sup>1</sup>, Andre Schneider<sup>1</sup>, Hannes Rotzinger<sup>1,2</sup>, Martin Weides<sup>3</sup> and Alexey V. Ustinov<sup>1,2</sup>

Quantum simulation is one of the most promising near term applications of quantum computing. Especially, systems with a large Hilbert space are hard to solve for classical computers and thus ideal targets for a simulation with quantum hardware. In this work, we study experimentally the transient dynamics in the multistate Landau-Zener model as a function of the Landau-Zener velocity. The underlying Hamiltonian is emulated by superconducting quantum circuit, where a tunable transmon qubit is coupled to a bosonic mode ensemble comprising four lumped element microwave resonators. We investigate the model for different initial states: Due to our circuit design, we are not limited to merely exciting the qubit, but can also pump the harmonic modes via a dedicated drive line. Here, the nature of the transient dynamics depends on the average photon number in the excited resonator. The greater effective coupling strength between qubit and higher Fock states results in a quasi-adiabatic transition, where coherent quantum oscillations are suppressed without the introduction of additional loss channels. Our experiments pave the way for more complex simulations with qubits coupled to an engineered bosonic mode spectrum.

npj Quantum Information (2023)9:61 ; <https://doi.org/10.1038/s41534-023-00731-7>

## INTRODUCTION

Noisy intermediate scale quantum (NISQ) devices, although imperfect, can have an advantage over classical computers at certain tasks<sup>1,2</sup>. Especially, analog quantum simulators (AQS), have advanced drastically over the last decade and can now tackle problems that are hard to solve for classical computers<sup>3,4</sup>. This is largely owed to the simplicity of their concept: in contrast to gate-based quantum computing, analog devices directly emulate a Hamiltonian of interest and thereby mimic all of its properties. Since they lack the flexibility and accuracy of a digital quantum computer, AQS are best suited to study universal effects, which are more or less resistant to small perturbations<sup>1</sup>. Therefore, open quantum systems are an appealing target for analog simulation, particularly, because they are also hard to model with both classical<sup>5</sup> and gate-based quantum computers<sup>6</sup>.

One such system is the multistate Landau-Zener model. It describes the interaction of an excitation at a time-dependent energy level with at least one other state or mode spectrum. Examples are the underlying Hamiltonian models for molecular collisions<sup>7</sup> and chemical reaction dynamics<sup>8</sup>. It is also ubiquitous in many artificial quantum devices, which have generated a broad research interest in recent years. In experimental studies on super-<sup>9–11</sup> and semiconducting qubits<sup>12,13</sup>, or nitrogen-vacancy centers in diamond<sup>14,15</sup> a Mach-Zehnder-like interference effect was exploited for quantum state preparations. The transient dynamics of the Landau-Zener model was also studied experimentally<sup>11,16–18</sup>, albeit only for two-state systems. In contrast, various theoretical works on the topic focus on the more complex multistate Landau-Zener model<sup>19–22</sup>. In particular, the time evolution of the system's state and its dependence on the mode spectrum are of great interest there.

In this work, we study the transient dynamics of the multistate Landau-Zener model of a superconducting quantum circuit. A tunable transmon qubit is used to realize a time-dependent

energy state. An artificial spectral environment is formed by four harmonic oscillators which are implemented as lumped element microwave resonators. We study the time evolution of the system as a function of the Landau-Zener velocity  $v$ , i.e., the speed at which the energy level separation bypasses the narrow spectral bath. In circuit, we are not limited to exciting the system via the qubit, but can also pump the harmonic modes directly. This allows us to investigate the qubit's time evolution for various initial states, and, in particular, as a function of the average photon number in the system. In our experiments, we observe coherent oscillations of the qubit population. For low average photon numbers, we compare our findings with numerical QuTiP simulations. For a strongly driven bosonic bath the transient dynamics gradually changes from a coherent oscillating to an adiabatic transition of the mode ensemble. We identify the  $\sqrt{n}$ -enhancement of the coupling strength<sup>23</sup> between the qubit and resonators with the number of photons  $n$  in the system as the underlying cause.

## RESULTS

### Implementation of the simulator

The Hamiltonian of the multistate Landau-Zener model reads

$$\frac{\hat{H}_{LZ}}{\hbar} = \frac{vt}{2} \hat{\sigma}_z + \sum_n \left( \omega_n \hat{a}_n^\dagger \hat{a}_n + g_n \hat{\sigma}_x \left( \hat{a}_n^\dagger + \hat{a}_n \right) \right), \quad (1)$$

where  $\hat{\sigma}_{x,z}$  are the Pauli-Operators of a two-level system with a time-dependent frequency of  $vt$ ,  $\hat{a}_n$  is the annihilation operator of the  $n$ th bosonic mode with a frequency of  $\omega_n$ , and  $g_n$  is the coupling strength of the  $n$ th bosonic mode to the two-level system. An implementation of this system with superconducting devices is straightforward, due to their tailored functionality and the good control over all circuit parameters. Figure 1a displays a micrograph of our simulation device. We use a tunable transmon

<sup>1</sup>Institute of Physics, Karlsruhe Institute of Technology, Karlsruhe, Germany. <sup>2</sup>Institute for Quantum Materials and Technologies, Karlsruhe Institute of Technology, Eggenstein-Leopoldshafen, Germany. <sup>3</sup>James Watt School of Engineering, University of Glasgow, Glasgow, UK. ✉email: alexstehli@gmail.com

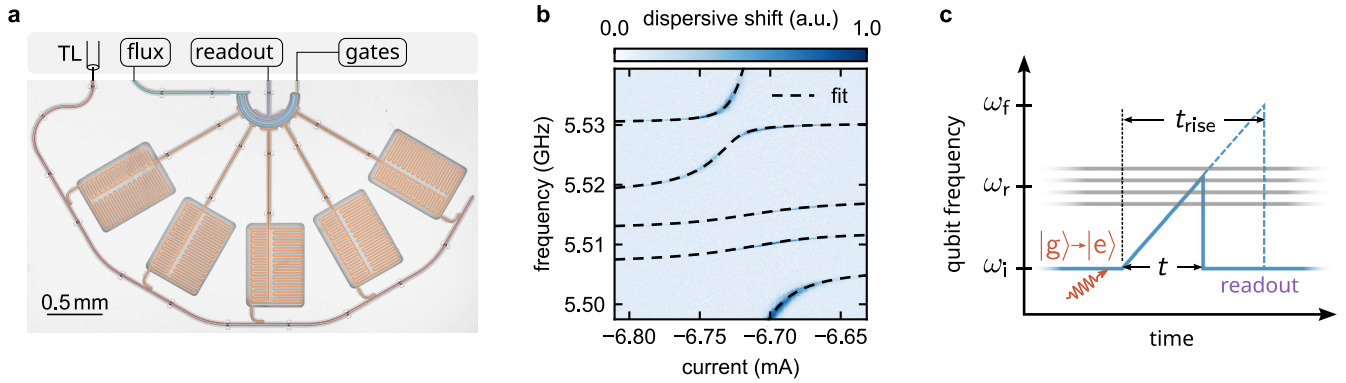


**Fig. 1 Characterization of the quantum simulator and simulation scheme.** **a** Micrograph of the simulation device. An ensemble of five lumped element resonators (orange) with a dedicated input line (red) is coupled capacitively to a transmon qubit (blue). We achieve fast tunability using an impedance matched flux bias line (cyan) coupled to the SQUID of the qubit. DC and AC current biases, respectively generated by a current source and AWG, are combined with a bias tee. Qubit gates are admitted via a dedicated drive port (yellow). A  $\lambda/4$ -resonator (purple) is employed for the dispersive measurement of the qubit state. **b** Two-tone spectroscopy of the avoided level crossings between the first qubit transition and bosonic modes. The coupling coefficients are extracted from a fit to the mode spectrum, see black dashed lines. They are in the same order as the frequency spacing between the harmonic modes. **c** At the start of the quantum simulation, the qubit frequency  $\omega_q$  (blue line) is tuned to  $\omega_i$ . Here, the system's initial state is prepared, shown for a  $\pi$ -pulse to the qubit. Thereafter follows a linear increase of the qubit frequency for a certain time  $t$ . We stop the qubit frequency sweep by returning the qubit to  $\omega_i$ , where dispersive state readout is performed. The qubit population along the trajectory is determined by repeating this process for different values of  $t$  up to a maximum rise time  $t_{\text{rise}}$ , where  $\omega_q = \omega_f$ .

qubit to approximate the two level system with a time-dependent energy transition, i.e., the leading term in the Hamiltonian. An impedance matched flux bias line coupled to the SQUID of the qubit enables fast control of the qubit frequency. At the working point, the qubit is tunable over a frequency range of up to  $\sim 400$  MHz. This is partially limited by the bias tee employed to combine AC and DC current biases, see Supplementary Methods. The qubit has an anharmonicity of  $a/2\pi = 241$  MHz and a rather large decoherence rate of  $\Gamma_2 = 5 \mu\text{s}^{-1}$ , which is not limited by the energy decay rate  $\Gamma_1 = 0.2 \mu\text{s}^{-1}$ . Due to the steep qubit dispersion at the operation point, flux noise is a likely limiting factor. The bosonic modes in the model are emulated by several lumped element microwave resonators with frequencies situated at around 5.5 GHz and capacitively coupled to the qubit. Experimentally, we find that only four of the five resonators interact with the qubit, see Supplementary Methods for detailed information. Qubit readout is performed dispersively utilizing a  $\lambda/4$ -stripline resonator with a resonance frequency of 6.86 GHz.<sup>24,25</sup> Qubit gates are applied via a dedicated drive line. An additional input line coupled to the bath resonators allows for a direct spectroscopy of their transition frequencies and can be exploited in time domain experiments to directly apply microwave pulses to the bosonic modes.

Figure 1b shows a two-tone measurement of the coupled multi-mode system, in the single-photon manifold. Here, the qubit frequency is tuned in and out of resonance with the bosonic modes via a DC current bias applied to the flux coil. Thereby, several avoided level crossings are revealed, which we employ to extract the coupling coefficients between the qubit and resonators. The frequency spacing of the bosonic modes is of the same order as their coupling strength to the qubit. The extracted device parameters are summarized in Supplementary Table 1 and are also employed in the numerical simulation of the system.

The Landau-Zener model is directly emulated by the quantum hardware. Therefore, no complex driving scheme is needed to run the simulation. The analog simulation follows the simple algorithm of system state preparation, free time evolution as the qubit frequency is increased, and finally qubit state readout, see Fig. 1c. Due to experimental constraints, the qubit is initially flux biased to  $\omega_q = \omega_i$  rather than to zero-frequency, approximately 200 MHz below the bosonic modes' transitions. The Landau-Zener velocity is given by  $v = (\omega_f - \omega_i)/t_{\text{rise}}$ , where the final qubit frequency  $\omega_f$  is

reached after the time  $t_{\text{rise}}$ . In the experiment, both  $\omega_i$  and  $\omega_f$  are measured quantities, while  $t_{\text{rise}}$  is adjusted by the arbitrary waveform generator (AWG) used to tune the qubit frequency  $\omega_q$ . We determine the qubit population at several time steps along this trajectory. For state readout, the qubit is returned to  $\omega_i$ , halting the time evolution. The time resolution is limited to 1 ns by the AWG generating the tuning pulse.

### Multi-mode Landau-Zener model

For the first experiment discussed in this work, we prepare the system in the first excited state, i.e., the excited state of the qubit, by applying a weak  $\pi$ -pulse ( $\sim 140$  ns length). Thereby, we make sure that the time development is dominated by the dynamics of the Landau-Zener model, rather than rotations of the qubit state stemming from the preparation in a system non-eigenstate. Figure 2a displays the results of our analog quantum simulation, side by side with numerical QuTiP simulations<sup>26,27</sup>, see Fig. 2b. In the numerical simulations, we truncate the bosonic modes to the first two Fock states and omit energy relaxation and decoherence of the system.

Qualitatively, we observe that, independent of the rise time, the qubit retains its excited state population until it reaches the resonator ensemble. After scattering on the bosonic modes, coherent oscillations of the qubit population emerge. The oscillation frequency is proportional to the energy difference of the qubit and bath states<sup>9</sup>. Therefore, it is independent of the coupling coefficients and solely depends on the velocity  $v$  and increases with time. The oscillation amplitude decreases with time, i.e., for increasing qubit frequency. We emphasize that this effect is not introduced by the limited life-, and coherence time of the simulation device. Rather, it is how the system converges to a static state achieved in the limit of  $t_{\text{rise}} \rightarrow \infty$ . We confirm the good quantitative agreement of numerics and experiment in a trace-wise comparison for several different rise times, see Fig. 2c. In the experiment, we have to account for a small offset of 5.2 ns to  $t_{\text{rise}}$ , see methods section, likely caused by a distortion of the tuning pulse after traversing the microwave lines to the sample.

Figure 2d displays the final qubit population as a function of rise time, in good agreement with numerical simulations. A potential cause of the overshoot of the qubit population for short rise times is constructive Mach-Zehnder interference<sup>9</sup>, which can occur due

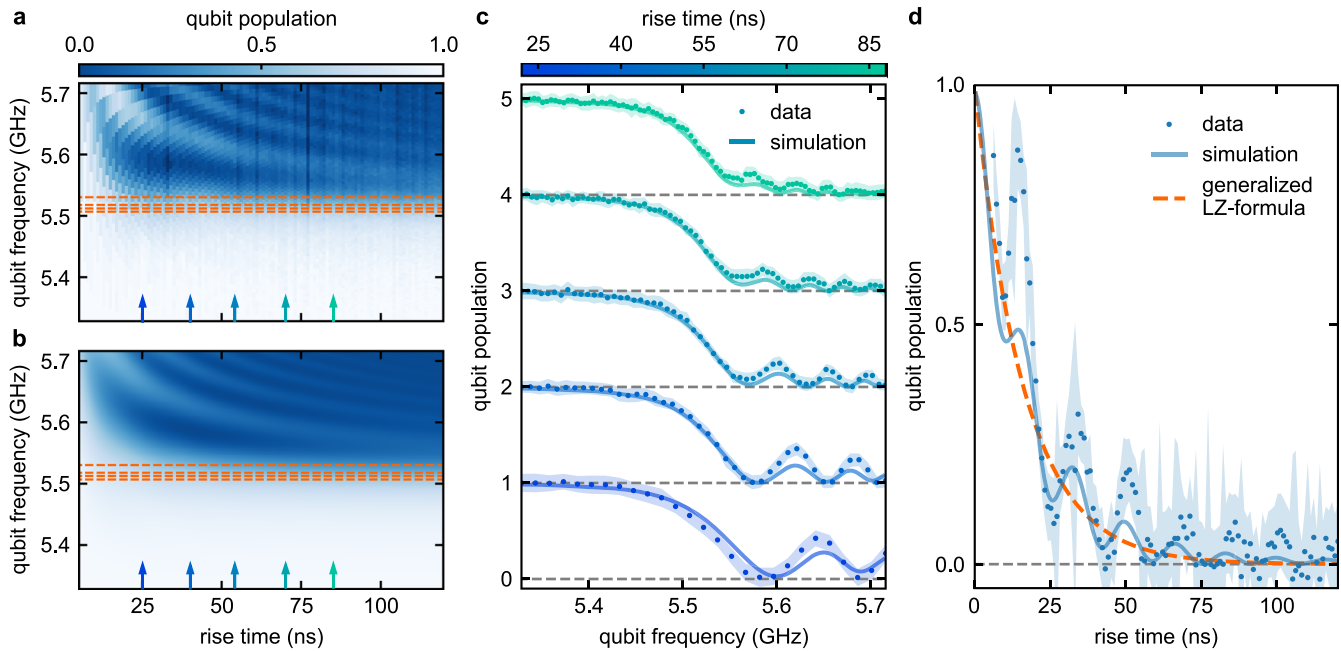


**Fig. 2** Transient dynamics in the multistate Landau-Zener model with an initially excited qubit. **a** Quantum and **b** numerical simulation of qubit population as a function of the qubit frequency  $\omega_q(t) = \omega_i + vt$  and rise time  $t_{\text{rise}} = (\omega_q - \omega_f)/v$  with the Landau-Zener velocity  $v$ . During the transition of the resonator ensemble (frequencies indicated by dashed orange lines), the population of the initially excited qubit undergoes a steep drop, followed by coherent oscillations with diminishing amplitude. This is especially apparent for long rise times. **c** Quantitative comparison of the experiment (dots) and numerical simulation (lines) for different rise times, indicated by blue arrows in **b**. Shaded areas indicate the standard deviation of the qubit population. Neighboring traces are shifted by 1 to improve visibility. **d** Final qubit population as a function of the rise time  $t_{\text{rise}}$ . Oscillations persist in measurement and simulation, nevertheless, the final qubit population is well approximated by the generalized Landau-Zener formula, see Eq. (2).

to the finite time needed to return the qubit frequency to  $\omega_i$ . We also compare our results with the generalized Landau-Zener formula<sup>28–30</sup>, which predicts a qubit population of

$$P_q = \prod_n \exp\left(-\frac{2\pi}{v} g_n^2\right). \quad (2)$$

for  $t_{\text{rise}} \rightarrow \infty$ . Each avoided level crossing can be interpreted as a beamsplitter for incoming photons<sup>9</sup>. Therefore, multiple crossings consecutively reduce the probability of the photon remaining in the qubit. Apart from the remnants of coherent oscillations in the measurement, our data are in agreement with the analytical formula. As predicted, the qubit remains in the excited state for  $t_{\text{rise}} \rightarrow 0$ , with the final state exponentially approaching the ground state in the adiabatic limit of  $t_{\text{rise}} \rightarrow \infty$ .

### Excited ensemble

Due to the dedicated drive line for the resonators, we can also pump the bosonic modes, rather than exciting the qubit. Thereby, their roles are reversed and the qubit, this time initially in the ground state, acquires (a fraction of) a photon from the populated mode during the transit. Since we cannot easily prepare the resonators in a Fock state, we apply a short drive pulse to one of the resonators. Thereby, it is prepared in a superposition state including higher levels, where the average photon number depends on the duration  $t_p$  of the pump pulse. Since  $t_p$  is lower than the resonators' decay rates  $\kappa$  across all presented experiments, the pump does not result in a coherent state in the excited oscillator.

Figure 3 displays the quantum (a–d) and numerical simulation (e–h) of the qubit population during the transition of resonator ensemble, one of which is excited. The pump pulse duration in the presented experiments was chosen as  $t_p = 80$  ns. In the numerical simulation, the bosonic mode was initialized in a one-photon Fock state to reduce the complexity of the calculation. Once again,

coherent oscillations of the qubit population emerge after its frequency traverses the bath. Here, the amplitude of the oscillations strongly depends on the initial state of the system. This is particularly clear in the picture of a chain of beamsplitters, where the survival probability of an injected photon increases when injected at a later stage. Furthermore it also explains the shift of the center of mass of the oscillation towards larger  $t_{\text{rise}}$  for a higher frequency of the initially excited resonator.

What happens if we now increase the average photon number in the excited resonator? Figure 3i shows the qubit population in dependence on the average photon number  $\langle n \rangle$  in the lowest frequency resonator  $b_1$  and for  $t_{\text{rise}} = 50$  ns. Here, we change  $\langle n \rangle$  by varying the duration  $t_p$  of the pump tone. Comparing with Fig. 3a, a higher population of the resonator initially leads to more pronounced oscillations with a larger amplitude. For very long pump tones the behavior changes to an increasingly adiabatic transition of the avoided level crossing. In the Jaynes-Cummings model, which is the basis of our simulator, the matrix element between a Fock state with photon number  $n$  and the qubit ground state scales with  $\sqrt{n}^{23}$ . The Landau-Zener tunneling probability scales with the square of this matrix element, see Eq. (2), which in turn corresponds to a faster (smaller Landau-Zener velocity  $v$ ), more adiabatic transit. A direct comparison with numerical simulations proves challenging, due to the complex initial state of the pumped resonator and the large Hilbert space of the system. However, we can qualitatively reproduce the time evolution of the qubit population in a drastically simplified version of the system, comprising only two resonators, see Supplementary Discussion.

### DISCUSSION

In this work, we experimentally investigated the time evolution of the multistate Landau-Zener model using a superconducting

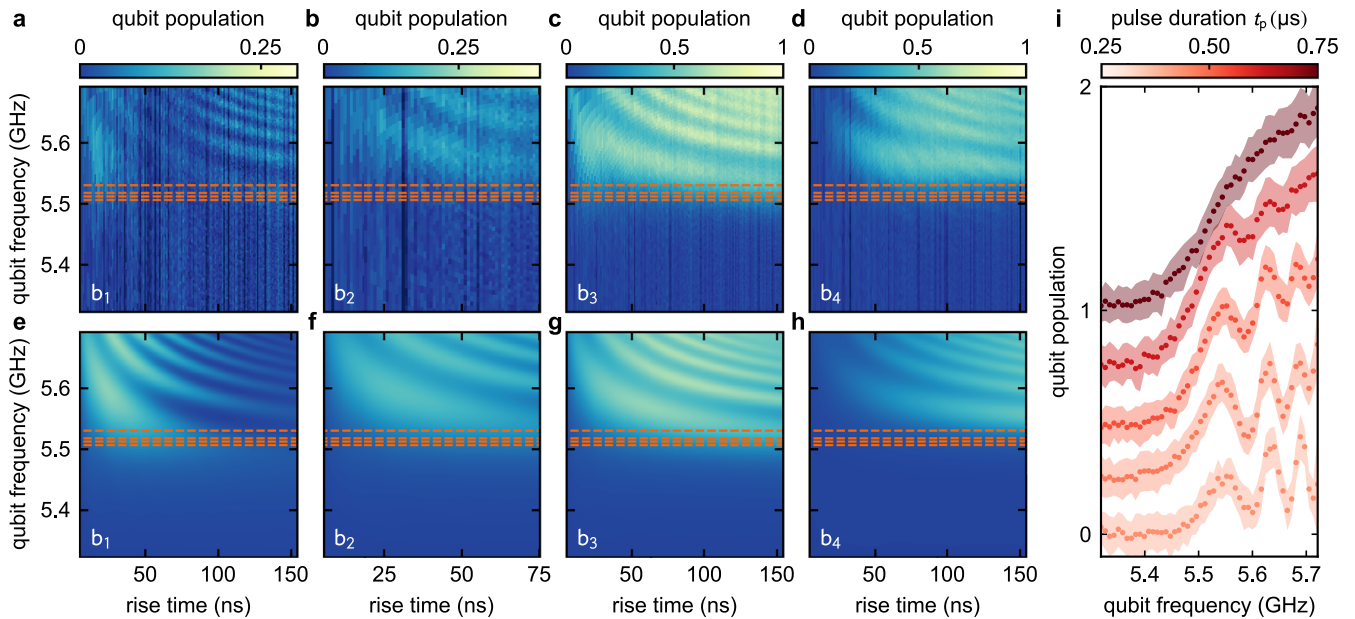


**Fig. 3 Qubit population dynamics with an excited resonator mode.** The qubit starts in the ground state and transitions the bosonic modes, one of which is excited. Each column of the panels corresponds to a different initial state, where the resonators are excited in ascending order ( $b_i$  for the  $i$ th resonator). In the experiment **a–d**, a single resonator is prepared in a state with a low average population. **e–h** QuTiP simulation of the dynamics (compare **a** to **e**, etc.). We find coherent oscillations of the qubit population. As expected from a series of beamsplitters, the amplitude depends strongly on the excited resonator, i.e., where the photon is injected in the beamsplitter setup. **i** Transient dynamics for  $t_{\text{rise}} = 50$  ns for a larger average photon number in resonator  $b_1$ . Shaded areas indicate the standard deviation of the qubit population. Neighboring traces are shifted by 0.25 to improve visibility. By increasing the duration  $t_p$  (shown for 250, 300, 400, 550, and 750 ns) of the pump pulse higher Fock states contribute to the dynamics of the system. The  $\sqrt{n}$ -scaling of the effective coupling strength between qubit and resonator with the photon number  $n$  of the respective Fock state increases the Landau-Zener tunneling probability, see Eq. (2). Initially, this results in a greater oscillation amplitude and a larger final value of the qubit population after the transit, but gradually shifts towards an adiabatic transition. For  $t_p = 750$  ns, the coherent oscillations of the qubit population are fully suppressed and the qubit is (approximately) in the excited state upon reaching  $\omega_i$ .

quantum simulator. The focus of this study was the transient dynamics of the qubit population in the vicinity of several bath resonators forming a spectral environment. By changing the Landau-Zener velocity  $v$  and the initial state of the system we observed coherent oscillations of the qubit population, which subside towards large  $v$  where the transition becomes adiabatic. In contrast to previous studies of the model, our simulator allows for a preparation of higher excited states of the participating bosonic modes. For a larger average photon number  $\langle n \rangle$ , the transit of the avoided level crossings gradually becomes adiabatic, which is the result of an effectively larger coupling strength  $g \propto \sqrt{n}$  between the qubit and the  $n$ th Fock state of the excited resonator. Throughout the paper, we validate the results of the quantum experiments with numerical QuTiP simulations. Our implementation of an engineered spectral environment inspires future efforts towards emulating the dynamics of open quantum systems with superconducting quantum circuits. For example, it offers a promising approach to realize a quantum simulator of the spin boson model<sup>31</sup> with a tailored spectral function and, with the help of the additional drive tones, explore it in the ultra-strong coupling regime<sup>32,33</sup>.

## METHODS

### Dispersive measurement of the qubit population

As described in the main text, we determine the qubit state via the dispersive shift of the readout resonator. Since our measurement setup lacks a quantum-limited amplifier, each data point is pre-averaged 500 times on the data acquisition card. This is repeated 25 times to calculate the standard deviation of the mean. Additionally, we had to calibrate the position of the resonator for ground and excited state. Especially, time dependent

fluctuations of the resonator frequency would otherwise prove detrimental. Therefore, the measurement sequences for each time trace include two additional points: For the first, we measure the dispersive shift after a  $\pi$ -pulse was applied to the qubit, which gives a reference point for the excited state. Second, the qubit frequency is tuned along the trajectory through the resonator ensemble and its state is measured after tuning it back to  $\omega_i$ . Since no excitation pulse is applied this gives a reference for the ground state. In the IQ-plane, we project all other data points in the sequence onto the connection line between the two reference measurements. The (effective) qubit population is then given by

$$P_q = \frac{x_i - x_g}{x_e - x_g}, \quad (3)$$

where  $x_i$  is the position of point  $i$  along the line, and  $x_{g/e}$  denotes the position of ground/excited state. The standard deviation is calculated from Gaussian error propagation.

### Offset calibration

We calibrate the offset of our time traces in the measurement by comparison with the numerical simulations. Here, we minimize the mean squared error between each data point and its corresponding point in the numerical simulation, as a function of a time and frequency offset to the qubit population. We find the lowest deviation for a shift of 5.2 ns and 2.4 MHz of the quantum simulation with respect to the numerical results.

### DATA AVAILABILITY

The data that support the findings of this study are available from the corresponding author upon reasonable request.

## CODE AVAILABILITY

The underlying code for this study is not publicly available but may be made available to qualified researchers at reasonable request from the corresponding author.

Received: 25 February 2023; Accepted: 13 June 2023;

Published online: 24 June 2023

## REFERENCES

1. Preskill, J. Quantum Computing in the NISQ era and beyond. *Quantum* **2**, 79 (2018).
2. Arute, F. et al. Quantum supremacy using a programmable superconducting processor. *Nature* **574**, 505–510 (2019).
3. Bernien, H. et al. Probing many-body dynamics on a 51-atom quantum simulator. *Nature* **551**, 579–584 (2017).
4. Zhang, J. et al. Observation of a many-body dynamical phase transition with a 53-qubit quantum simulator. *Nature* **551**, 601–604 (2017).
5. Mostame, S. et al. Emulation of complex open quantum systems using superconducting qubits. *Quantum Inf. Process.* **16**, 44 (2017).
6. García-Pérez, G., Rossi, M. A. C. & Maniscalco, S. IBM Q Experience as a versatile experimental testbed for simulating open quantum systems. *npj Quantum Inf.* **6**, 1 (2020).
7. Child, M. S. *Molecular collision theory* (Courier Corporation, 1996).
8. Nitzan, A. *Chemical dynamics in condensed phases: relaxation, transfer and reactions in condensed molecular systems* (Oxford university press, 2006).
9. Oliver, W. D. et al. Mach-Zehnder Interferometry in a Strongly Driven Superconducting Qubit. *Science* **310**, 1653–1657 (2005).
10. Sillanpää, M., Lehtinen, T., Paila, A., Makhlin, Y. & Hakonen, P. Continuous-time monitoring of Landau-Zener interference in a cooper-pair box. *Phys. Rev. Lett.* **96**, 1–4 (2006).
11. Berns, D. M. et al. Amplitude spectroscopy of a solid-state artificial atom. *Nature* **455**, 51–57 (2008).
12. Petta, J. R., Lu, H. & Gossard, A. C. A Coherent Beam Splitter for Electronic Spin States. *Science* **327**, 669–672 (2010).
13. Ota, T., Hitachi, K. & Muraki, K. Landau-Zener-Stückelberg interference in coherent charge oscillations of a one-electron double quantum dot. *Sci. Rep.* **8**, 5491 (2018).
14. Childress, L. & McIntyre, J. Multifrequency spin resonance in diamond. *Phys. Rev. A* **82**, 033839 (2010).
15. Fuchs, G. D., Burkard, G., Klimov, P. V. & Awschalom, D. D. A quantum memory intrinsic to single nitrogen-vacancy centres in diamond. *Nat. Phys.* **7**, 789–793 (2011).
16. Yoakum, S., Sirko, L. & Koch, P. M. Stueckelberg oscillations in the multiphoton excitation of helium Rydberg atoms: Observation with a pulse of coherent field and suppression by additive noise. *Phys. Rev. Lett.* **69**, 1919–1922 (1992).
17. Zenesini, A. et al. Time-Resolved Measurement of Landau-Zener Tunneling in Periodic Potentials. *Phys. Rev. Lett.* **103**, 090403 (2009).
18. Huang, P. et al. Landau-Zener-Stückelberg Interferometry of a Single Electronic Spin in a Noisy Environment. *Phys. Rev. X* **1**, 011003 (2011).
19. Vitanov, N. V. Transition times in the Landau-Zener model. *Phys. Rev. A* **59**, 988–994 (1999).
20. Zueco, D., Hänggi, P. & Kohler, S. Landau-Zener tunnelling in dissipative circuit QED. *New J. Phys.* **10**, 115012 (2008).
21. Orth, P. P., Imambekov, A. & Le Hur, K. Universality in dissipative Landau-Zener transitions. *Phys. Rev. A* **82**, 1–5 (2010).
22. Orth, P. P., Imambekov, A. & Le Hur, K. Nonperturbative stochastic method for driven spin-boson model. *Phys. Rev. B* **87**, 119–123 (2013).
23. Tavis, M. & Cummings, F. W. Exact Solution for an N-Molecule-Radiation-Field Hamiltonian **170** (1968).
24. Blais, A., Huang, R. S., Wallraff, A., Girvin, S. M. & Schoelkopf, R. J. Cavity quantum electrodynamics for superconducting electrical circuits: An architecture for quantum computation. *Phys. Rev. A* **69**, 62320 (2004).
25. Wallraff, A. et al. Strong coupling of a single photon to a superconducting qubit using circuit quantum electrodynamics. *Nature* **431**, 162–167 (2004).
26. Johansson, J., Nation, P. & Nori, F. QuTIP: an open-source Python framework for the dynamics of open quantum systems. *Comput. Phys. Commun.* **183**, 1760–1772 (2012).
27. Johansson, J., Nation, P. & Nori, F. QuTIP 2: a Python framework for the dynamics of open quantum systems. *Comput. Phys. Commun.* **184**, 1234–1240 (2013).
28. Shytov, A. V. Landau-zener transitions in a multilevel system: an exact result. *Phys. Rev. A* **70**, 2–4 (2004).

29. Wubs, M., Saito, K., Kohler, S., Hänggi, P. & Kayanuma, Y. Gauging a quantum heat bath with dissipative Landau-Zener transitions. *F* **97**, 2–5 (2006).
30. Saito, K., Wubs, M., Kohler, S., Kayanuma, Y. & Hänggi, P. Dissipative Landau-Zener transitions of a qubit: bath-specific and universal behavior. *Phys. Rev. B* **75**, 214308 (2007).
31. Leggett, A. J. et al. Dynamics of the dissipative two-state system. *Rev. Mod. Phys.* **59**, 1–85 (1987).
32. Ballester, D., Romero, G., García-Ripoll, J. J., Deppe, F. & Solano, E. Quantum simulation of the ultrastrong-coupling dynamics in circuit quantum electrodynamics. *Phys. Rev. X* **2**, 1–6 (2012).
33. Leppäkangas, J. et al. Quantum simulation of the spin-boson model with a microwave circuit. *Phys. Rev. A* **97**, 052321 (2018).

## ACKNOWLEDGEMENTS

Cleanroom facilities use was supported by the KIT Nanostructure Service Laboratory (NSL). We are grateful to Alexander Shnirman for the fruitful discussions. This work was supported by the European Research Council (ERC) under the Grant Agreement No. 648011, Deutsche Forschungsgemeinschaft (DFG) projects INST 121384/138-1FUGG and WE 4359-7, EPSRC Hub in Quantum Computing and Simulation EP/T001062/1, and the Initiative and Networking Fund of the Helmholtz Association. A.S. acknowledges support from the Landesgraduiertenförderung Baden-Württemberg (LGF), J.D.B. acknowledges support from the Studienstiftung des Deutschen Volkes. T.W. acknowledges support from the Helmholtz International Research School for Teratronics (HIRST).

## AUTHOR CONTRIBUTIONS

A.St., J.D.B., M.W., and A.V.U. conceived the experiment. A.St. fabricated the samples. A.St., T.W., A.Sc., and J.D.B. carried out the experiments. A.S. performed the numerical QuTIP simulations. All authors were involved in discussions of the results and contributed to the writing of the manuscript. M.W. and A.V.U. supervised the project.

## FUNDING

Open Access funding enabled and organized by Projekt DEAL.

## COMPETING INTERESTS

The authors declare no competing interests.

## ADDITIONAL INFORMATION

**Supplementary information** The online version contains supplementary material available at <https://doi.org/10.1038/s41534-023-00731-7>.

**Correspondence** and requests for materials should be addressed to Alexander Stehli.

**Reprints and permission information** is available at <http://www.nature.com/reprints>

**Publisher's note** Springer Nature remains neutral with regard to jurisdictional claims in published maps and institutional affiliations.



**Open Access** This article is licensed under a Creative Commons Attribution 4.0 International License, which permits use, sharing, adaptation, distribution and reproduction in any medium or format, as long as you give appropriate credit to the original author(s) and the source, provide a link to the Creative Commons license, and indicate if changes were made. The images or other third party material in this article are included in the article's Creative Commons license, unless indicated otherwise in a credit line to the material. If material is not included in the article's Creative Commons license and your intended use is not permitted by statutory regulation or exceeds the permitted use, you will need to obtain permission directly from the copyright holder. To view a copy of this license, visit <http://creativecommons.org/licenses/by/4.0/>.

© The Author(s) 2023